AGU PUBLICATIONS

JGR

Journal of Geophysical Research: Oceans

RESEARCH ARTICLE

10.1002/2017JC013263

Key Points:
- Extreme low light requirement for algae growth
- Unique measurements of under-ice algae growth under ~2 m of snow and sea ice
- A change in snow optical properties allows algae growth via temperature-driven snow metamorphosis

Correspondence to:
K. Hancke,
kasper.hancke@niva.no

Citation:
Hancke, K., Lund-Hansen, L. C., Lamare, M. L., Højlund Pedersen, S., King, M. D., Andersen, P., & Sorrell, B. K. (2018). Extreme low light requirement for algae growth underneath sea ice: A case study from Station Nord, NE Greenland. *Journal of Geophysical Research: Oceans*, *123*, 985–1000. https://doi.org/10.1002/2017JC013263

Received 11 JUL 2017
Accepted 16 JAN 2018
Accepted article online 19 JAN 2018
Published online 6 FEB 2018

Extreme Low Light Requirement for Algae Growth Underneath Sea Ice: A Case Study From Station Nord, NE Greenland

Kasper Hancke[1,2], Lars C. Lund-Hansen[1,3], Maxim L. Lamare[4], Stine Højlund Pedersen[3,5], Martin D. King[4], Per Andersen[6], and Brian K. Sorrell[1]

[1]Department of Bioscience, Aquatic Biology, Aarhus University, Aarhus, Denmark, [2]Now at Norwegian Institute for Water Research (NIVA), Research Centre for Coast and Ocean, Oslo, Norway, [3]Department of Bioscience, Arctic Research Centre, Aarhus University, Aarhus, Denmark, [4]Department of Earth Sciences, Royal Holloway University of London, Surrey, UK, [5]Department of Biological Sciences, University of Alaska Anchorage, Anchorage, AK, USA, [6]NIRAS, Ceres Allé 3, Aarhus, Denmark

Abstract Microalgae colonizing the underside of sea ice in spring are a key component of the Arctic foodweb as they drive early primary production and transport of carbon from the atmosphere to the ocean interior. Onset of the spring bloom of ice algae is typically limited by the availability of light, and the current consensus is that a few tens-of-centimeters of snow is enough to prevent sufficient solar radiation to reach underneath the sea ice. We challenge this consensus, and investigated the onset and the light requirement of an ice algae spring bloom, and the importance of snow optical properties for light penetration. Colonization by ice algae began in May under >1 m of first-year sea ice with ~1 m thick snow cover on top, in NE Greenland. The initial growth of ice algae began at extremely low irradiance (<0.17 μmol photons m^{-2} s^{-1}) and was documented as an increase in Chlorophyll *a* concentration, an increase in algal cell number, and a viable photosynthetic activity. Snow thickness changed little during May (from 110 to 91 cm), however the snow temperature increased steadily, as observed from automated high-frequency temperature profiles. We propose that changes in snow optical properties, caused by temperature-driven snow metamorphosis, was the primary driver for allowing sufficient light to penetrate through the thick snow and initiate algae growth below the sea ice. This was supported by radiative-transfer modeling of light attenuation. Implications are an earlier productivity by ice algae in Arctic sea ice than recognized previously.

1. Introduction

Ice algae are a substantial contributor to Arctic primary production creating a food source for ice-associated zooplankton and amphipods (Arrigo, 2014; Soreide et al., 2010), both of which are key contributors to the Arctic food web. The timing of the ice algae bloom has implications for food availability and quality for ice-associated zooplankton, and for the success rate of zooplankton hatching (Leu et al., 2010, 2011). Moreover, ice algae play a significant role for the Arctic carbon cycle and sequestration, and are important as a carbon export pathway from surface waters to the deep ocean (Assmy et al., 2013; Boetius et al., 2013; Fernandez-Mendez et al., 2014; Glud et al., 2007). Also in the Antarctic, landfast sea ice algae are important contributors to primary production and carbon turnover (McMinn et al., 2010).

Ice algae are typically abundant when there is sufficient irradiance underneath the sea ice for photosynthesis and growth, and their biomass can be considerable, compared to phytoplankton in Arctic coastal and ocean ecosystems (Leu et al., 2015, and references herein). However, little is known about the early timing of ice algae blooms, especially the threshold irradiance required to trigger early ice algae colonization and growth, including how well ice algae are acclimated to very low light levels (Hawes et al., 2012; Robinson et al., 1997; Thomas & Dieckmann, 2009). The minimum requirement of light to support photosynthetic net growth has been estimated theoretically to account to ~10 nmol photon m^{-2} s^{-1} (Raven et al., 2000). Under sea ice, only a few empirical data sets and estimates of the minimum light requirement for growth of ice algae exist due to logistical and technical challenges. The lowest current estimate is 0.36 μmol photons m^{-2} s^{-1} (Mock & Gradinger, 2000). This estimate has been suggested an underrate due to the scattering nature of the ice-water interface (Ehn & Mundy, 2013). Other *in situ* studies reports of a photon flux requirement of 2–9 μmol photons m^{-2} s^{-1} for net growth of ice algae (Gosselin et al., 1986; Horner & Schrader, 1982; Leu et al., 2010; Rysgaard et al., 2001).

Light availability underneath sea ice is regulated by radiative-transfer of solar radiation through the ice and overlying snow cover (Gosselin et al., 1990; Marks & King, 2014; Thomas & Dieckmann, 2009). Despite an often thicker layer of ice than snow, snow thickness is usually the most important in regulating the availability of light for ice algae, because of its much higher light attenuation properties.

The scattering properties of snow are regulated by its density, grain size, and grain shape. Grain size is affected by snow temperature gradients via metamorphism of snow (Marks & King, 2014). On sea ice, temperature gradients within the snowpack typically create a vapor pressure gradient from the relatively warm bottom upward to the colder layers in connect with the atmosphere. Such vapor gradients lead to an increase in snow grain size and a decrease in the optical scattering cross section of the snow, again leading to a decrease in light attenuation (Lamare et al., 2016; Libois et al., 2013). It has been suggested that ~40 cm of snow cover is enough to prevent algal growth (Campbell et al., 2014; Mundy et al., 2007).Until recently, it has been anticipated that below such snow covers, little biological activity was occurring due to the absence of light.

In this study, we provide evidence of an early onset of ice algae growth at very low light conditions, below >1 m of snow and 1 m of sea ice. Further, we provide modeled data of the photon flux penetrating a thick snow cover and underlying sea ice, and argue that the optical properties of snow are regulating the light availability underneath sea ice early in the spring. We aimed to study the light requirement for ice algae growth, and to quantify the minimum photon flux needed to support net growth of ice algae and initiate the spring colonization. Further, we test the idea that optical properties of snow are an important factor controlling the light availability underneath sea ice. Implications are that Arctic sea ice algae may bloom much earlier than often anticipated with consequences for Arctic primary production and carbon flux in ice covered regions.

2. Materials and Methods

2.1. Site Description and Sample Collection

The study presented here provides the first sea ice algae data from the Wandel Sea near the newly established Villum Research Station (VRS), located at the Danish military base "Station Nord" in far North East Greenland (Figure 1). Data were collected between 16 April and 24 May 2015 as part of the large international Arctic Science Partnership research campaign, coordinated by the Arctic Research Center, Aarhus University, Denmark.

Data were collected at a main station (termed 1C) approximately every third day, and along a ~20 km transect (1A to 1E) stretching NW from the shoreline of the research station into the Wandel Sea. The inner part of the Wandel Sea is relatively shallow stretching from the shoreline to the shelf drop, with water depth of <200 m. Water depths at the investigated stations are listed in Table 1. The Wandel Sea meets a complex of large fjords to the south west, consisting of Danmarks Fjord, Hagens Fjord and Independence Fjord, while bordering the Arctic Ocean at the Northeast (Dmitrenko et al., 2016). Sea ice completely covers the fjord complex during winter, in part by First-Year (FYI) and in part by Multi-year (MYI) sea ice, with FYI typically dominating along the shores and MYI the interior of the basin. The present study includes only land-fast first-year sea ice samples.

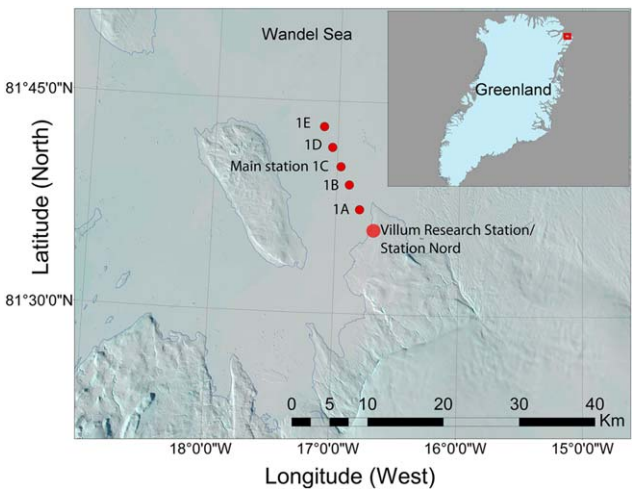

Figure 1. Map of sampling area, including the 5 sampling stations (1A to 1E) located across a transect stretching ~20 km to the north west from the shore line outside the Villum Research Station and Station Nord, a Danish military station. The map is based on a MODIS AQUA (NASA) image from 25 April 2015, downloaded from www.dmi.dk.

The thickness of snow cover was measured with a manual snow-depth probe at each sea-ice coring site. Snow-depth observations were also collected in the surrounding area of site 1C in an orthogonal transect (~700 m in total length). In addition, the snow-cover thickness was estimated automatically using a sonic ranging sensor (Campbell Scientific SR50A) at a land-based monitoring station 2 km from the Villum Research Station. Observations of the physical properties of the snowpack were collected in snow pits dug at 1C on 5 May and 16 May including snow temperature (handheld digital thermometer), snow density (Snow-Hydro 100cc density cutter), and snow grain size, i.e., the longest dimension of the crystal (snowmetrics.com crystal card and magnifier).

Table 1
Station Positions, Ice Type, Thickness of Ice and Snow and Water Physics

Station #	Lat. N	Long. W	Ice type #	Ice thickness[a] cm	Snow thickness[b] cm	Snow thickness from transect[c] cm	UIW temp °C	UIW sal PSU	Water depth m
1A	81.623	16.807	FYI	115	98.9 ± 5.3		−1.1	19.5	20
1B	81.652	16.896	FYI	118	91.6 ± 3.1		−1.2	19.5	58
1C	81.673	16.969	FYI	110	95.0 ± 4.4	95.4 ± 7.0 (5 May) 94.1 ± 10.3 (16 May)	−1.2	19.4	73
1D	81.696	17.043	FYI	114	99.2 ± 3.1		−1.1	19.3	75
1E	81.72	17.115	FYI	145	98.7 ± 3.4		−1.1	19.3	87

[a]n = 3. [b]n = 10. [c]n= 198.

Temperature profiles through the snow and ice pack were measured continuously every hour using a thermistor string buoy, also called an ice mass balance (IMB) buoy, developed and built by the Scottish Association for Marine Science (SAMS) institute (Jackson et al., 2013). The thermistor string was positioned at the main station 1C on 5 May and measured until the end of May. The thermistor consisted of a 4 m long string equipped with digital temperature chip sensors for each 2.0 cm. It was positioned to measure a vertical distance from 40 cm above the air-snow interface, down through the snowpack, through the sea ice, and reaching 30 cm below the ice-water interface. The sensor string was placed through a 4.5 cm hole carefully drilled from the top of the snow to the base of the sea ice. After placement, the drill hole was allowed to refreeze. Via an incorporated heating element in each temperature sensor, the instrument was able to resolve the material interfaces to within a few centimeters (e.g., air-snow and ice–water boundaries) even under isothermal conditions. The top end of the string was connected to a data logger and control unit, while a weight was attached to the distal end keeping it a straight line to below the sea ice.

Sea ice cores were collected using a Mark II Coring system with a diameter of 9 cm (Kovacs Enterprises). They were collected for chemical and biological sampling after removing the snow cover from the sea ice. A minimum of three cores were collected at each site, of which the lower 5 cm was collected for further analyses (e.g., chlorophyll, cell number, and nutrients). Cores were transported in dark cold bags to the laboratory within three hours after sampling, to maintain the *in situ* temperature. In the laboratory ice samples were melted slowly in the dark during 24 h, diluted 1:1 with Whatman GF/F filtered sea water, sampled immediately under the sea ice. Samples of Under-Ice Water (UIW) were collected from 1 m beneath the sea ice using a small handheld water sampler (temperature and salinity are shown in Table 1).

To investigate if the ice algae community was light limited, a perturbation experiment that cleared the snow cover (2x2 m) from the sea ice was initiated on 24 April at the main station (1C). Owing to strong winds and precipitation, snow had to be repeatedly removed from the manipulated site on 1 May and 6 May. Triplicated samples of sea ice and sea water were collected from the snow-cleared site in a similar manner to the undisturbed stations, with a distance of approximately 0.5m.

2.2. Optical Measurements

Incident downwelling and upwelling Photosynthetically Active Radiation (PAR) above the snowpack and under the sea ice were measured continuously at the main station (1C) during the campaign, using flat cosine-corrected PAR sensors (LiCor 191 above and LiCor 192 below) connected to a Campbell CR10X data logger. The under-ice sensor was positioned through a 9 cm diameter core hole penetrating both the snow pack and sea ice. The sensor was positioned 3 cm below the underside of the sea ice 15 cm away from the core hole. After positioning the sensor, the drill hole was carefully filled with the drill core and packed with snow. The instruments were undisturbed during the field campaign. Down- and upwelling solar (global) radiation (CNR4 Net Radiometer, Kipp & Zonen) were also measured at the Villum Research Station using an automatic weather station (established by Asiaq, Greenland Survey on behalf of the Department of Environmental Science/Danish Centre for Environment and Energy [DCE], and operated by Aarhus University).

Albedo of the snow pack was calculated as the ratio of upwelling PAR to downwelling PAR. The detection limit of the PAR sensors was 0.15 μmol photons m^{-2} s^{-1}.

Downwelling spectral irradiance [$E_d(\lambda)$] was measured as a function of snow depth and underneath the sea ice from 320 to 950 nm with a 3.3 nm spectral resolution, using a spectroradiometer (RAMSES ACC-VIS, TriOS, Germany). Vertical profiles of downwelling spectral irradiance were measured through the snow pack after digging a snow-pit allowing for a vertical positioning of the spectral irradiance sensor, 30 cm 'inside' the southern wall of the snowpit, after characterizing the physical properties of the snow (France & King, 2012). The vertical resolution of the profiles was 5 to 20 cm following the snow layers with different densities. Measurements were started from the snow-ice interface working upward, ensuring that the snow layers above the instrument remained undisturbed. Profiles were measured on 7 May at solar noon.

Under-ice downwelling spectral irradiance was measured using a RAMSES sensor positioned 5 cm below the ice-water interface, 50 cm laterally from a core hole, positioned using a folding L-shaped metal 'arm' reaching through the hole and sideways underneath the sea ice. To minimize stray light from core holes, the RAMSES sensor was positioned through a narrow core hole (9 cm diameter) that was carefully drilled through both the windpacked snow and the sea ice below, with minimum disturbance of the area around the hole. The core hole was filled with ice and snow during measurements. During profiling and under ice irradiance measurements, the surface incident PAR was measured simultaneously using a small cosine-corrected quantum sensor (MQS-B, logged on a ULM-500 data logger, Walz, Germany). Only irradiance measurements that were sampled during constant surface irradiance conditions (<5% change) were collected. The RAMSES spectral irradiance sensor was freshly factory-calibrated for the campaign, and acted as the campaign standard for all the PAR sensors which were calibrated against this. Unfortunately, the RAMSES sensor filled with seawater after the measurements on May 7th, and failed thereafter.

Diffuse wavelength-specific vertical attenuation coefficients were calculated ($K_{d(\lambda)}$, m^{-1}) according to (Kirk, 1994):

$$K_{d(\lambda)} = \frac{\ln\left(E_{dz1(\lambda)}/E_{dz2(\lambda)}\right)}{z2-z1} \quad (1)$$

where $E_{dz1(\lambda)}$ and $E_{dz2(\lambda)}$ represent downwelling irradiance at two different depths (z) in the snow/ice column, respectively.

2.3. Photosynthetic Measurements

To investigate if the sampled ice algae were viable and photosynthetically active, we applied a sensitive technique to study the instant photosynthetic performance, i.e., the Pulse Amplitude Modulated (PAM) fluorescence technique. Here we used a Walz PhytoPAM variable fluorometer (System I, Walz, Effeltrich, Germany,(Schreiber et al., 1986)), equipped with a highly sensitive Photomultiplier-Detector (PM-101P, Walz). Initially, the sampled ice cores were brought into the laboratory in dark cool bags, as ice samples for chemical analysis (see above). However, upon arrival in the laboratory (within a few hours after sampling) variable fluorescence yield as originating from active photosynthesis, could not be detected. Hereafter, a tent camp was established on the ice allowing rapid and protected processing of ice algal samples, a temperature-controlled measuring environment (air temperature was kept around zero degrees in the tent), and shade from the strong incident irradiance. The tent camp was established at the main station (1C) on the 16 May and ice algae were collected from the lower 1 cm of sampled cores around noon. Ice crystals containing algae were transferred immediately to a standard plastic cuvette (with 4 clear sides), warmed just enough for the ice crystals to melt by the palm of a hand (wearing disposable powder-free vinyl gloves), and as soon as the samples became liquid they were placed inside the PAM incubation chamber and acclimatized in the dark (3 min). After instrument gain was optimized, repeated measurements of photosynthetic quantum yields were successfully taken. The maximum quantum yield of charge separation (Φ_{max}) was calculated from the dark-acclimated fluorescence (F_o) and the maximum fluorescence (F_m) after a saturation light pulse, as $(F_m - F_o)/F_m$ (Genty et al., 1989). F_o and F_m measures were corrected for background non-photosynthetic fluorescence using a 'blank' sample, which was obtained by a 0.2 μm filtered sub-sample of the original sample. For details on the measuring protocol see (Hancke et al., 2015).

2.4. Laboratory Analyses

The chlorophyll *a* (Chl *a*) concentration (mg m^{-3}) in ice cores was measured from the sea-water-diluted samples filtered onto GF/F glass fiber filters (Whatman) extracted in 5 mL 96% ethanol within 24 h (dark, 4°C). The concentration was determined in triplicate using a pre-calibrated fluorometer (Turner Designs

TD-700) (Lorenzen, 1966; Lund-Hansen et al., 2016). The same procedure was used for Chl *a* measurements of the UIW, except that these were not diluted prior to filtering.

Dominating algae groups were identified from light-microscopy analyses using a Palmer Maloney chamber, on samples collected from FYI cores and from UIW preserved in LUGOL (neutral, 1% final solution).

Concentrations of $[NO_3^-]$ and $[NO_2^-]$, collectively termed $[NO_3^-]$, were determined as NO on a NOx analyzer (Model 42C, Thermo Environmental Instruments Inc.) after reduction to NO in hot Vanadium Chloride (Braman & Hendrix, 1989). Concentrations of $[PO_4^{3-}]$ and $[NH_4^+]$ were determined by standard colorimetric methods (Grasshoff et al., 1999) on a Shimadzu UV-1800 spectrophotometer.

2.5. Modeling

Numerical radiative-transfer calculations of downwelling PAR through the snow and sea ice were undertaken using the Tropospheric Ultraviolet and Visible Radiation Model (TUV-snow) (Lee-Taylor & Madronich, 2002). The TUV-snow model is a coupled atmosphere/snow or sea ice model that uses the DISORT code (Stamnes et al., 1988) and is described fully in (Lee-Taylor & Madronich, 2002).

To model the field observations of PAR at station 1C, a layer of snow was modeled on a first-year sea ice layer, with an underlying optically thick layer representing the seawater under the sea ice. The layers of snow and sea ice were further split into multiple layers with all the same optical properties for the snow and sea ice respectively. Two modeling approaches were adopted. In the first scenario, the snow was consecutively given the optical properties of three snow types previously characterized by the authors (Lamare et al., 2016; Marks & King, 2014): cold polar snow, coastal windpacked snow and melting snow. A 1m thick cover of snow, representing the average thickness of the snowpack at station 1C, was defined on a 1 m thick sea ice. In the second scenario, the sea ice optical properties remained the same but the thickness of the snowpack was set to 91 and 110 cm, to fit the observations. The value of the light scattering cross section of the snowpack, σ_{scatt}, was varied over a wide range to represent snow metamorphism. The value of σ_{scatt} is inversely proportional to the snow grain size (Libois et al., 2013), and metamorphism of the snow tends to increase the snow grain size (Warren, 1982) and thereby decrease the value of σ_{scatt}.

The light scattering and absorption in each sea ice and snow simulation are constrained in the model by an asymmetry factor, a wavelength independent scattering cross section, σ_{scatt}, a wavelength dependent absorption cross section, σ_{abs}^+, and the sea ice/snow density and thickness (Lamare et al., 2016; Lee-Taylor & Madronich, 2002). A first year sea ice layer was modeled with a mass density of 800 kg m^{-3}, a scattering cross section of 0.15 m^2 kg^{-1} and a fixed asymmetry parameter *g* of 0.98, based on field values parametrized in Marks and King (2014). A density of 400 kg m^{-3} and a fixed asymmetry parameter *g* of 0.89 were used to model the covering snow layer. The value of the scattering cross section of the snow was set to 1.25 m^2 kg^{-1} for melting snow, 7.50 m^2 kg^{-1} for coastal windpacked snow and 20.0 m^2 kg^{-1} for melting snow (Lamare et al., 2016; Marks & King, 2014). The scattering cross section was then varied between 1 m^2 kg^{-1} and 25 m^2 kg^{-1}, in 5 m^2 kg^{-1} steps for the second modeling experiment.

The wavelength dependent absorption cross section of ice was obtained from (Warren & Brandt, 2008) for the snow and sea ice. A mass-ratio of 1 ng g^{-1} of black carbon was added to the sea ice and snow, as small quantities of black carbon are likely to be found in snow and sea ice in polar regions (e.g., Doherty et al., 2010). To represent the seawater under the sea ice, a fixed wavelength independent albedo of 0.1 was used. The atmospheric parameters used in the model are the same to that described in detail in (Lamare et al., 2016).

The downwelling PAR throughout the snow and sea ice column was calculated as:

$$PAR = \int_{\lambda=400nm}^{\lambda=700nm} I(\lambda) d\lambda, \tag{2}$$

with $I(\lambda)$, the downwelling monochromatic irradiance and λ, the wavelength. The snow and sea ice were subdivided into 1 cm thick layers, apart from the 10 layers between atmosphere and snow, snow and ice, and ice and seawater, which were 1 mm thick. The downwelling PAR was calculated for each layer throughout the snow and sea ice.

3. Results and Discussion

3.1. Initiation of Ice Algae Growth Under Extremely Low Light Conditions

Here we document the initial phase of an ice algae spring bloom underneath thick landfast sea ice in Arctic NE Greenland, and provide evidence that ice algae spring growth may initiate at an irradiance of less than 0.17 μmol photons m^{-2} s^{-1}, much lower than previously measured (Ehn & Mundy, 2013; Gosselin et al., 1986; Leu et al., 2010; Mock & Gradinger, 2000). We also present data to support the idea that a change in optical properties of snow can lead to an increased irradiance availability under the sea ice from a decrease in the optical scattering cross section of the snow, using radiative transfer model calculations.

During the campaign period from April to June the Wandel Sea was permanently covered by approximately 1 m of snow and 1 m of sea ice (Table 1 and Figure 2). Until early June the snow thickness only decreased marginally, and the air temperature was well below 0 °C (average for April was −19.2 °C, for May −13.2 °C, and for June +1.2 °C, Figure 2b).

During this period, incident solar radiation increased by ~4 fold, as the noon incident PAR increased from ~300 to ~1,200 μmol photons m^{-2} s^{-1} (corresponding to 13 and 69 mol photons m^{-2} d^{-1}, Figure 2a).

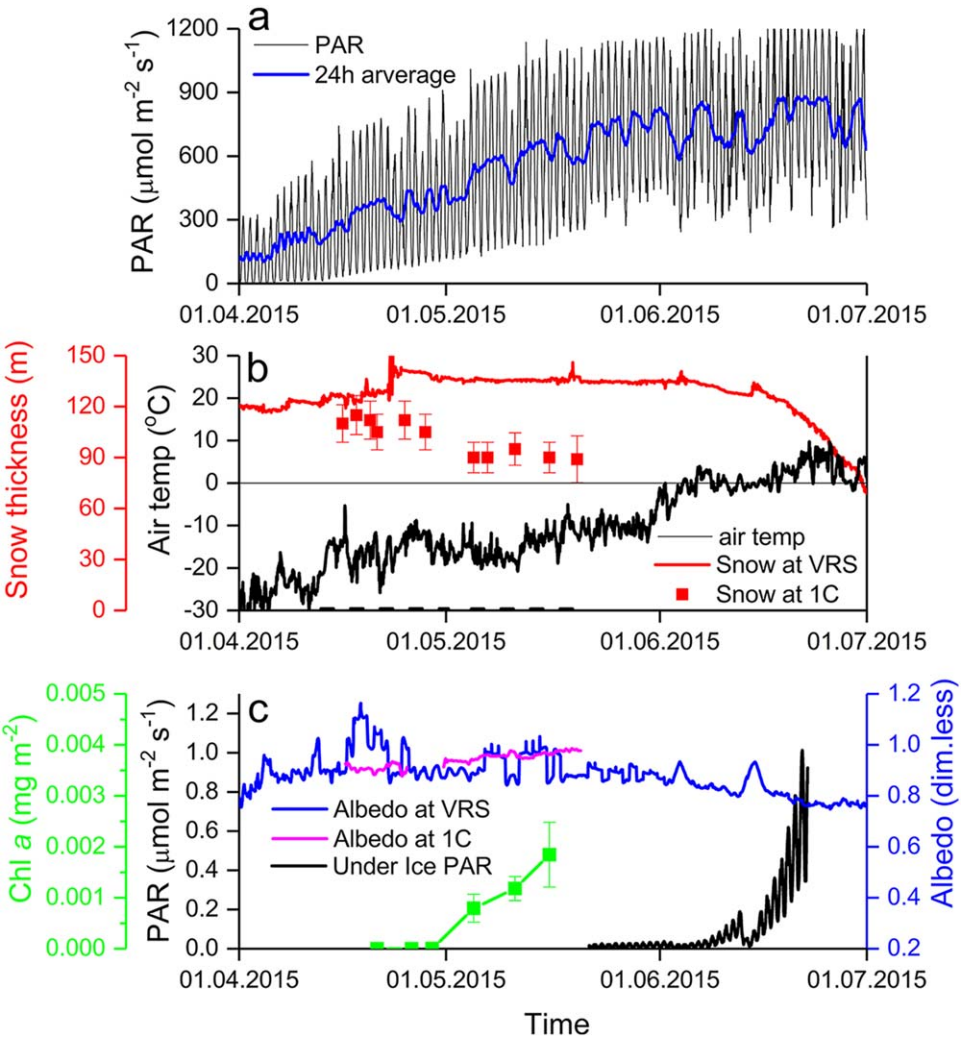

Figure 2. (a) Surface incident PAR (sampled every 30 min, 24 h running average in blue); (b) snow thickness at the Villum Research station (VRS, red line) and at station 1C (red squares, ± S.D.), air temperature (black line); and (c) surface albedo at the VRS (blue line) and at station 1C (magenta line), under ice PAR (black), and under-ice Chl *a* (green squares, ± S.D.). Data at the Villum Research Station were collected on land.

Correspondingly, the maximum solar elevation angle increased from 13 to 30 degrees (a solar zenith angle change of 77° to 60°), from early April to late May.

The albedo in the PAR wavelength range was almost unchanged during this same period (average ~0.9, Figure 2c). The under-ice irradiance was below the detection limit of the installed PAR sensor at the monitoring station 1C (0.15 μmol photons m^{-2} s^{-1}) until May 21, and did not exceed 0.2 μmol m^{-2} s^{-1} until June 16 (Figure 2c). On May 5, a PAR intensity of 0.17 μmol m^{-2} s^{-1} was measured underneath the sea ice after an intrusive spectral irradiance sensor (RAMSES, TriOS) was sent through a drill hole (see below).

The first detection of ice algae Chl *a* significantly different from zero ($P = 0.037$) was on May 5 (0.001 mg m^{-2}), despite a nearly unchanged thickness in snow and sea ice cover the preceding month (Figure 2c). After this date, Chl *a* increased continuously as measured on 11 and 16 May, and which was interpreted as robust evidence of algae net growth and the very first stage of an ice algae bloom and colonization. This was a surprising result, as light availability under the sea ice was extremely low at this time, and the photon flux reaching the base of the sea ice was efficiently reduced by the thick snow and ice cover.

It seems likely that a light intensity of 0.17 μmol photons m^{-2} s^{-1}, as observed at noon on 5 May was enough to support the net growth of algae, and thus exceeded the compensation irradiance of the ice algae community. Due to unavoidable sampling artefacts, 0.17 μmol photons m^{-2} s^{-1} is even likely an overestimate of the true irradiance below an undisturbed surface. Hence, the maximum daily integrated irradiance underneath the sea ice was extremely low. Irradiance intensities above the compensation point (i.e., the irradiance at which gross primary production equals community respiration) marks the initial start of an algae bloom (Marra, 2004; Raven et al., 2000). To our knowledge, the lowest estimate of ice algae compensation irradiance is 0.36 μmol photons m^{-2} s^{-1}, suggested by Mock and Gradinger (2000). This estimate has in fact been suggested to underestimate the compensation irradiance (Leu et al., 2015) due to effects of light scattering at the base of the sea ice (Ehn & Mundy, 2013). In general, ice algae are some of the most extreme low-light adapted phototrophic species but in situ measurements are rare due to experimental and logistical challenges (Thomas & Dieckmann, 2009). Commonly, values in the range of 2–9 μmol photons m^{-2} s^{-1} are considered compensation irradiances for ice algae (Gosselin et al., 1986; Horner & Schrader, 1982; Leu et al., 2010). In extreme low light environments in the Antarctic, benthic microalgae have been reported photosynthetically active at less than 1 μmol photons m^{-2} s^{-1} (Robinson et al., 1995). In deep water, extreme low-light adapted red macroalgae have a minimum light requirement of 1.5 μmol photons m^{-2} s^{-1} (Pritchard et al., 2013). The most extreme low-light adapted phototrophic organisms reported is a crustose coralline red macroalga that has been found growing at a depth of 274 m near the Bahamas, at a calculated midday PAR irradiance of less than 0.02 μmol photons m^{-2} s^{-1} (Littler et al., 1985, 1986, 1991). It has, however, been questioned whether its metabolism is supported by mixotrophy (Raven et al., 2000). What we suggest here is thus a new minimum light requirement for ice algae net growth.

Under Arctic landfast sea ice, in regions with less snow, ice algae colonization typically begins earlier in the season depending on latitude, as reviewed by Leu et al. (2015) and references therein. Field data from Resolute Bay (Arctic Canada) show a consistent relationship between development of ice algae Chl *a* concentrations and the thickness of the snow pack. Ice algae colonization began in the middle of March for <10 cm of snow, in the beginning of April when snow cover was between 10 cm and 20 cm, and in the middle of April at snow depths >20 cm (data compiled from multiple studies from 1985 to 2011; Leu et al., 2015). Snow thickness <40 cm has been suggested as a required threshold for algae growth to occur (Campbell et al., 2015; Mundy et al., 2007), and most ice algae studies have been conducted with conditions of only a few centimeters of snow on the sea ice (e.g., Hawes et al., 2012; Leu et al., 2010; Mundy et al., 2007). To our knowledge, there are no previous scientific reports of ice algae abundance or thickness of snow from further north in East Greenland than Young Sound (74.3°N). However, Station Nord is known to have higher winter precipitation than typical High Arctic regions, partially explained by the presence of the Northeast Water (NEW) Polynya of the east coast (Day et al., 2013; Krabill et al., 2000). The Danish military Sirius dog sled patrol reports that >1 m of snow is not unusual for the region around Villum Research Station.

To verify that the observation of the early abundance of sea ice algae Chl *a* (Figure 2c) was not restricted to the monitoring station 1C, ice cores and under-ice-water (UIW) were collected from 5 stations across a 20 km transect on May 11th and 14th (Figures 1 and 3a). The ice cores showed consistent concentrations of Chl *a* in the lower 3 cm of the core, between 0.001 and 0.002 mg m^{-2}, along the transect. These values are

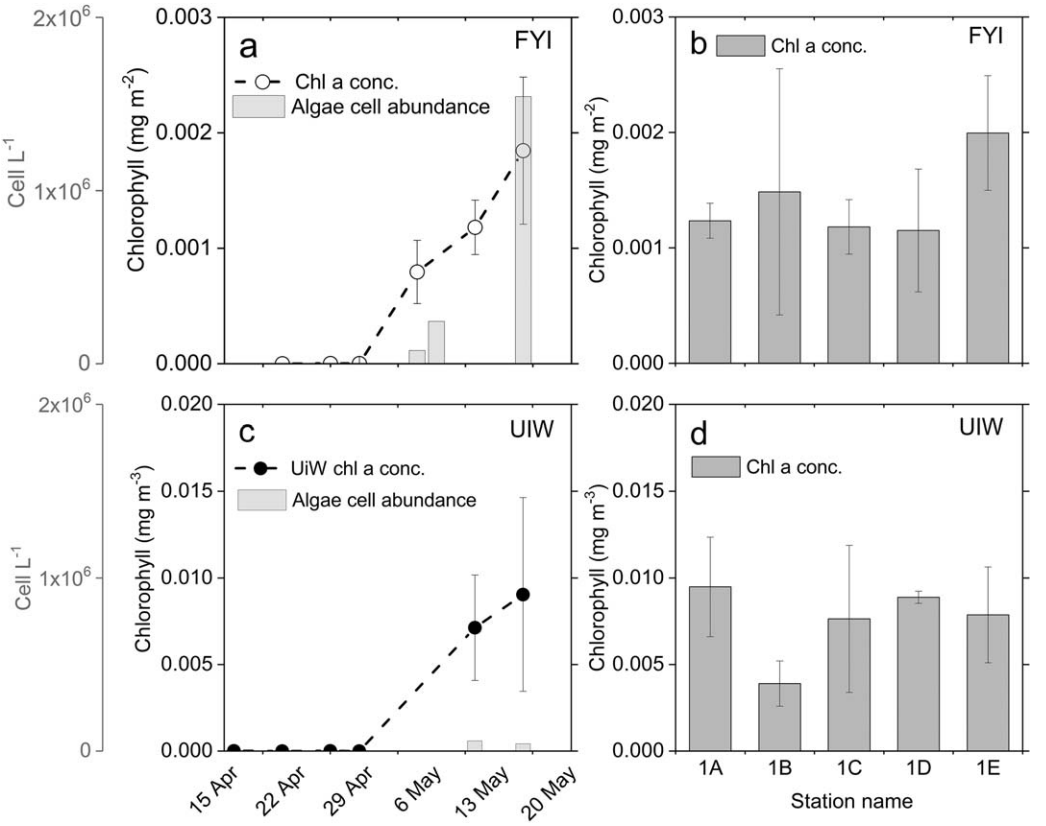

Figure 3. Chl *a* in first year ice (FYI) and in sea water underneath the ice (UIW): (a) Chl *a* and algae cell abundance in FYI as a function of time (Chl *a* data from Figure 2c), and (b) Chl *a* concentration at 5 stations across a ~20 km long transect from station A to E on 11 May (Station E was sampled on 14 May, n = 3). c) Chl *a* and algae cell abundance in under-ice-water (UIW) as a function of time and d) across the transects (n = 3). Error bars are standard deviation.

significantly different from zero ($P < 0.05$, Figure 3b). Figure 3b shows that the trend of the time series data at station 1C was an accurate characterization of the trend in the region rather than a local phenomenon. In the under-ice-water (UIW), the Chl *a* concentration indicates an initial growth, as it increased from below detection to 0.01 mg m^{-3} toward May 16 (Figure 3c). The trend is, however, not statistically significant. The UIW observations were nevertheless supported by similar findings across the 20 km transect, showing similar concentrations of Chl *a* to Station 1C (0.005-0.01 mg m^{-3}, Figure 3d). Cell abundance obtained from Lugol fixed samples further verified the presence of algae cells and the temporal development in the sea ice and the under-ice water samples (Figures 3a and 3c). The identity of the dominating algae species in the lower 3 cm of the sea ice are given in Table 2.

The concentrations of Chl *a* presented here are extremely low compared to previous published values. In East and West Greenland, ice algae Chl *a* concentrations typically reach a seasonal maximum around 1 mg m^{-2} (Glud et al., 2007; Hawes et al., 2012; Mikkelsen et al., 2008; Rysgaard et al., 2001). These values are low in a Pan-Arctic perspective, which typical shows seasonal peak concentrations near 20 mg m^{-2} (Leu et al., 2015, and references herein; Rysgaard & Glud, 2007). In the Canadian Arctic, seasonal peak values of >100 mg m^{-2} have occasionally been reported (e.g., Cota & Horne, 1989), and Chl *a* values of 150 to >300 mg m^{-2} are reported from Antarctic sea ice algae communities (McMinn et al., 2000; Palmisano & Sullivan, 1983).

It should be emphasized that it is highly unlikely that the identified chlorophyll concentration in this study is due to advection from an open water source, given the great distance (> 100 km) to the nearest open water (Northeast Water Polynya) and absence of ridges or cracks in the FYI (as observed from satellite data and ground observations). An oceanographic survey of the region during the same campaign reported relatively fresh water being present immediately below the ice (salinity of 16–21psu at 1–5 m), with no trace of

Table 2
Dominant Algae Groups and Inorganic Nutrient Concentrations in the Brine of the Lower 3 cm of the First-Year Old Sea Ice (FYI), and Inorganic Nutrients in the Under-Ice Water (UIW), n = 3

	Dominating algae groups[a] (%)			Nutrients, FYI (μmol L^{-1})				Nutrients, UIW (μmol L^{-1})			
	Flagellates	Dinoflagellates	Diatoms	NO_2+NO_3	NH_3	PO_4	Si	NO_2+NO_3	NH_3	PO_4	Si
29 Apr	-	-	-	0.65	5.3	0.1	2.4	0.9	0.4	0.4	2.3
5 May	99.6[b]	-	[c]	-	-	-	-	-	-	-	-
7 May	91	1.3[b]	7.7[d]	0.3 ± 0.1	1.1 ± 0.2	0.1 ± 0.03	-	-	-	-	-
11 May	-	-	-	0.7 ± 0.17	3.0 ± 0.4	0.1 ± 0.05	0.4	1.2	0.9	0.3	2.3
16 May	99.7	0.15[e]	0.15[c]	1.6	7.8	0.5	0.5	1.3	0.6	0.4	2.6

[a]Unidentified pico-algae were dominating (>70% cell abundance) in all FYI samples. Here the remaining groups in percent of total minus pico-algae, [b]Unidentified (excl. bacteria). [c]Traces of *Thalassiosira sp.*, [d]*Nitzschia closterium, N. longissima, Skeletonema costatum*, and unidentified, [e]*Prorocentrum spp, Protoperidinium* spp.

imported water masses (Dmitrenko et al., 2016). The fresh water presumably originated from previous summer snow/ice melt water and freshwater runoff from a nearby glacier.

Inorganic nutrients from the ice and under-ice water showed sufficient concentrations to support algae growth and there are no reasons to suspect that nutrient concentrations are limiting (Table 2). These values correspond to inorganic nutrient concentrations observed elsewhere in East Greenland, e.g., Young Sound (Rysgaard et al., 2001), but are lower than those typically found elsewhere in sea ice and under-ice water around Svalbard (Leu et al., 2010), and in the Canadian Arctic (Alou-Font et al., 2013; Mundy et al., 2007).

3.2. Light Attenuation and Requirement for Growth

Visible light attenuation in the snowpack was exponential in the bulk snow, giving e-folding depths of ~16 cm (K_d ~6 m^{-1}, Figures 4a and 4b). These findings are comparable to values found in Barrow, Alaska (France et al., 2012), and Ny-Ålesund, Svalbard (France et al., 2011). Visible light attenuation in the near surface region of the snowpack depends on the solar zenith angle and sky conditions (Simpson et al., 2002; Warren, 1982), and corresponding values of K_d are effectively phenomenological of the measurements.

During light attenuation measurements on 7 May under a clear sky around noon, the surface PAR was 750 μmol photons m^{-2} s^{-1}, the corresponding downwelling irradiance at the ice-snow interface <1 μmol photons m^{-2} s^{-1} (Figure 4a), and PAR under the ice 0.17 μmol photons m^{-2} s^{-1}. This corresponds to a transmission through the snow and ice layers of 0.023%, which is considerably lower than previously recorded in the presence of ice algae. Typical low recordings from similar latitudes but with less snow include minimum transmittance of ~0.5% measured in April in Ripfjorden, Svalbard (Leu et al., 2010), and a PAR transmittance of 1.1 to 3.2% during the spring bloom in the Canadian Arctic (Campbell et al., 2016). In the Arctic Ocean PAR transmittance of <1% has been recorded under 'thick ice' in spring (Assmy et al., 2017), while on average 9 ± 3% was recorded across 25 stations during summer in 2012 (Lund-Hansen et al., 2015). These all reports of algae growth under considerably more light under the sea ice than observed here.

In the snowpack, the downwelling attenuation coefficients (K_d) were between 5 and 15 m^{-1} (Figure 4b, e-folding depths of 20–67 cm) and consistent with previous records from the Arctic region, (France et al., 2011, 2012). Spectral irradiance available at different depths throughout the snow pack were measured for each density layer (Figure 4c), and show presence of light across the ultra-violet (UV, 300–400 nm), PAR (400–700 nm), and infrared regions (IR, 700–800 nm) of the spectrum. Light attenuation was lowest in the UV and blue-green part of the PAR spectrum (<500 nm) with increasing attenuation in the yellow-red part (>575 nm) and throughout the IR. The observed spectral shape of the attenuation agreed with previous observations of the optical properties of snow (France et al., 2012; Warren, 1982; Warren & Brandt, 2008). The spectral light availability below the sea ice was mostly restricted to the PAR wavelengths due to the strong attenuation of UV and IR light (Figures 4e and 4f). In the present study, undisturbed downwelling spectral irradiance could not be obtained closer to the snow-ice interface than 35 cm (for practical reasons). Spectral vertical attenuation was markedly lower in the ice than in the snow (Figure 4f). However, note that the integrated measure of the light attenuation across the 1 m thick sea ice includes 35 cm of snow on top. It should also be noted that the measured irradiance in the snow represents downwelling irradiance only

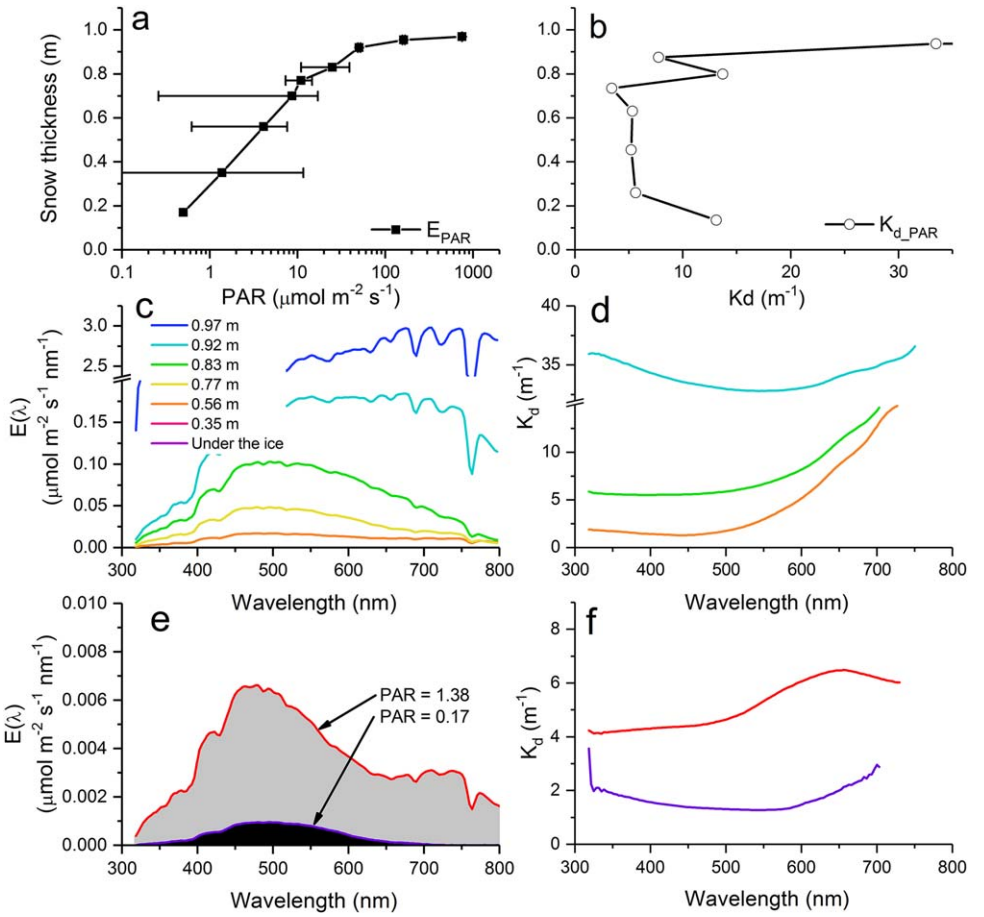

Figure 4. Measured spectral irradiance through the snow cover and under sea ice and the corresponding attenuation coefficients (K_d). (a) Profile of PAR (error bars are C.V); (b) profile of $K_{d,PAR}$; (c) E(λ) at different depth in the snow cover (see figure legend); and (d) correspond $K_{d(\lambda)}$(data represent lower depth). (e) E(λ) under the sea ice (purple) and 0.35 m above in the snow (lowest good measure) and (f) correspond $K_{d(\lambda)}$. Data are from station 1C, collected on May 7th at noon with a surface PAR of 750 μmol photons m^{-2} s^{-1}.

and thus underestimates the light availability for phototrophic and photochemical reactions as it does not include the upwelling irradiance. In highly scattering media as snow, upwelling irradiance can account for up to almost half of the available light scalar irradiance (Lee-Taylor & Madronich, 2002). However, under the ice in clear water, upwelling irradiance accounts for only a very minor fraction of the total, thus downwelling irradiance accurately represents the true light availability immediately below the ice. Inherently, light measurement beneath sea ice with algae underestimates the light availability to algae communities owing to the absorption of the light by algae themselves. These factors hinder empirically accurate measurement of light availability to ice-associated algae communities. However, in this case Chl *a* concentrations were extremely low and the above effect was assumed o be negligible. More importantly, the light availability to ice algae photosynthesis at the ice-water interface has been suggested to be severely underestimated from under ice measurements of downwelling irradiance, due to strong scattering of light in the skeletal layer of ice forming and hosting algae communities in the under ice environment (Ehn & Mundy, 2013). Whilst this suggestion was not documented experimentally in this study, the authors recognize the potential effect. On the contrary, the invasive light measurements obtained with the TriOs sensor likely overestimated the under-ice irradiance, as snow was removed and a hole drilled through the snow and ice to position the instrument under the sea ice.

3.3. Verification of a Viable and Photosynthetically Active Ice Algae Community

To investigate if the ice algae were light limited, and to verify that the observed algal community beneath the snow and sea ice was viable and photosynthetically active, a perturbation experiment was performed.

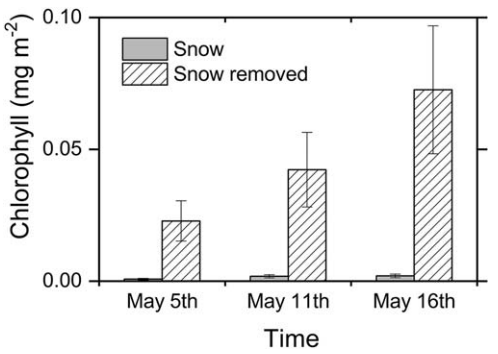

Figure 5. Effect on Chl *a* of a snow-removal perturbation experiment in first-year sea ice. Bars filled with diagonal lines represent samples collected where the ~1 m thick snow was removed from the sea ice forming a ~4 m^2 pit. Solid bars are Chl *a* sampled the same days at the nearby main site (1C). Snow was initially removed on April 24. The result demonstrates the potential for ice algae to grow and bloom in the absence of snow, which restrict the solar radiation from reaching through the sea ice. Error bars are standard deviation, n = 3 independed ice cores.

The snow cover was cleared from a 2x2 m patch of sea ice, and a pronounced effect on the Chl *a* concentration in the sea ice at the ice-water interface was observed (Figure 5). Removal of the snow allowed light to access the sea ice unattenuated, and thus light was only attenuated by the sea ice itself. There was a multifold increase in the Chl *a* concentration that increased steadily from when the perturbation experiment was initiated on April 24. By May 16 the Chl *a* concentration had increased 36 times relative to the untreated site. Two conclusions were drawn from the perturbation experiment: First, the algal community present beneath the sea ice was limited by light, not nutrients, and secondly, the ice algae were viable and physiologically active. Similar effects from other snow clearing experiments have been observed (Campbell et al., 2015; Lund-Hansen et al., 2014).

PAM fluorescence measurements verified that microalgae collected from the ice and UIW were viable and photosynthetically active. Measurements supported viable algae from the bottom of the sea ice showing a maximum quantum yield of 0.31 ± 0.031 (dimensionless, Figure 6), when cores were investigated in the field immediately after sampling. This provides evidence that the ice algae were growing and photosynthetically active under the ambient light conditions. Values are, however, at the lower end of the range of previous published photosynthetic quantum yields in Arctic ice algae (Hawes et al., 2012; Robinson et al., 1997; Rysgaard et al., 2001). In the under-ice water the maximum quantum yield was 0.13 ± 0.01 (Figure 6), which is low compared to optimal values for diatoms in laboratory suspensions and mixed pelagic populations (0.6-0.8; Hancke et al., 2008, 2015). For the perturbation experiments it was not possible to obtain measurements of the photosynthetic quantum yield on 16 May, unfortunately. The exact reason for this is not clear, but no reliable induction curves were measured, in contrast to FYI and UIW samples. However, the missing and low measures of the maximum quantum yields should be interpreted in context of an extremely low biomass (at detection limit of the instrument), harsh sampling conditions (>20 °C different between *in situ* and *ex situ* temperatures), and high irradiance at the top of the sea ice (>700 μmol m^{-2} s^{-1}). These conditions cannot be excluded as having a shocking effect on the fragile ice algae during sampling, even when great care was taken to prevent stress (e.g., shading of ice cores immediately after sampling, transport time of less than 5 min, and controlled temperature conditions). Nevertheless, the quantum yields compare well with values reported by Hawes et al. (2012) who found values of ~0.1 for ice algae at the initial stage of colonization, with a subsequent increase to ~0.5 when the algae bloom had established.

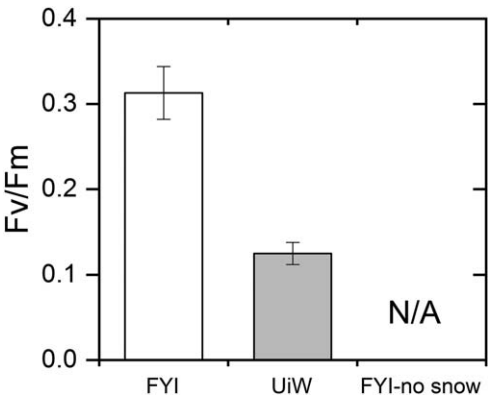

Figure 6. Maximum photosynthetic quantum yield (Φ_{PSII_max}) in dark-acclimated ice algae from First-Year Ice (FYI) and in Under Ice Water (UIW). Data were measured with a portable PAM fluorometer (PhytoPAM, Walz) within minutes after sampling of the ice cores, shaded from ambient light and temperature in a small tent. Samples are from Station 1C, 16 May around solar noon. No successful measurements were collected from the perturbation experiment (FYI-no snow). Error bars are standard deviation.

3.4. Snow Metamorphosis Driven by Temperature Gradients

Temperature profiles through the snow and ice pack were measured continuously every hour from 5 May until the end of May by the IMB buoy. Snow temperature showed a pronounced diel variation with minimum temperatures during night time and a maximum around noon (Figure 7). Most pronounced was the diel variation a few cm below the snow-air interface, showing the net result of air temperature and solar radiation heating of the surface snowpack. The depth in the snow at which the temperature was constant through the day became closer to the snow-ice interface with the progression of the season, from ~50 cm on 8 May, ~35 cm on 15 May, to ~20 cm on 19 May (Figure 7). This demonstrates a decrease in the insulation properties and increased wetting of the snowpack. There was no temperature gradient in the sea ice from the snow-ice to the ice-water interface during the entire measurement campaign, and the sea ice temperature was constant at −1.2 °C. The isothermal sea ice was confirmed from manual measurements of segments immediately after ice coring on several occasions (data not shown). The efficient insulation properties of the overlaying snow ensured

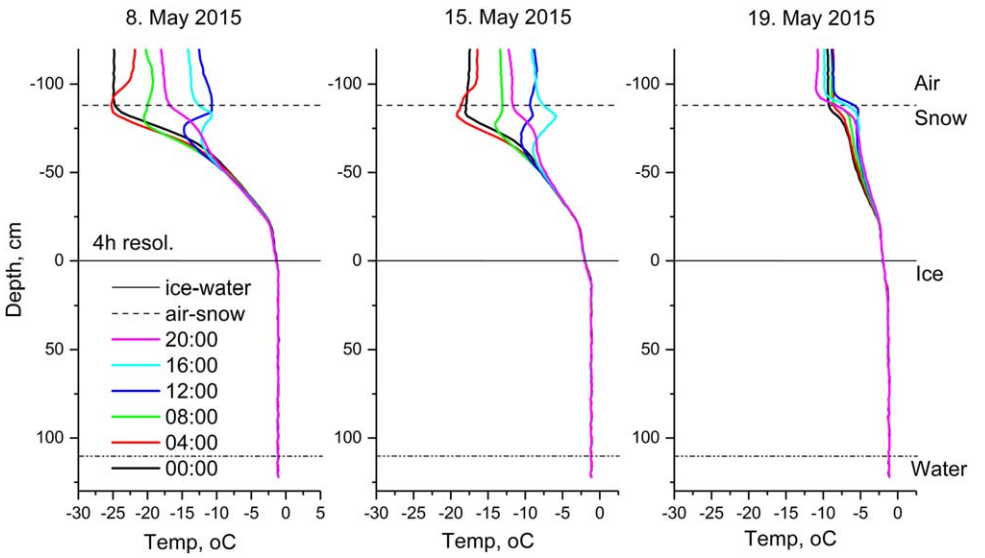

Figure 7. Temperature profiles in cross section through the snow and sea ice, showing air temperatures at the top and sea water temperature at the bottom. Profiles representing every 4 hours at three selected days illustrating how the snow pack is warming through May. The figure illustrates how solar heating is progressing increasing the snow temperature deeper in the snow pack over time, changing the temperature gradient within the snowpack. Y-axe refers to water depth in cm, negative numbers being above the ice-snow interface.

these stable physical conditions in the ice, and minimum freezing and thawing of the ice at the ice-water interface, during May.

The temperature profiles in Figure 7 overall demonstrated a strong temperature gradient showing an increase in temperature in direction from the top of the snow toward the snow-ice interface (Figure 7). This temperature gradient was confirmed from manual recordings in snow pits on 7 and 16 May (data not shown). Such conditions are optimal for snow metamorphism, i.e., a restructuring and reshaping of the snow crystal/grain in snowpacks (Colbeck, 1982). Temperature gradients in snow generate a vapor pressure gradient, which produces a flux of water vapor molecules upward to the relatively colder layers on the top. When the water vapor condenses on the over-lying snow crystals, it stimulates crystal growth and an increase in snow grain size and a decrease in snow density (LaChapelle, 1969). This effect is particularly strong when temperature gradients are larger than 1 °C per 10 cm of snow, as observed here during the beginning of May (Figure 7). Field data from the snow pits confirmed an increase in grain size and decrease in snow density, showing a 14% increase in overall grain size and a 25% decrease in bulk snow density (from 325.6 ± 91.4 kg m^{-1} to 244.8 ± 97.3 kg m^{-1}) between 7 and 16 May (10 days). Such an increase in grain size leads to a decrease in the optical scattering cross section and a concurrent decrease in the diffusive light attenuation properties of the snow (Lamare et al., 2016; Libois et al., 2013). Thus, a radiative-transfer model was introduced to assess if this change in the scattering cross section of the snow could explain the apparent increase in the light climate under the sea ice and supply the ice algae community with a sufficient photon flux for growth.

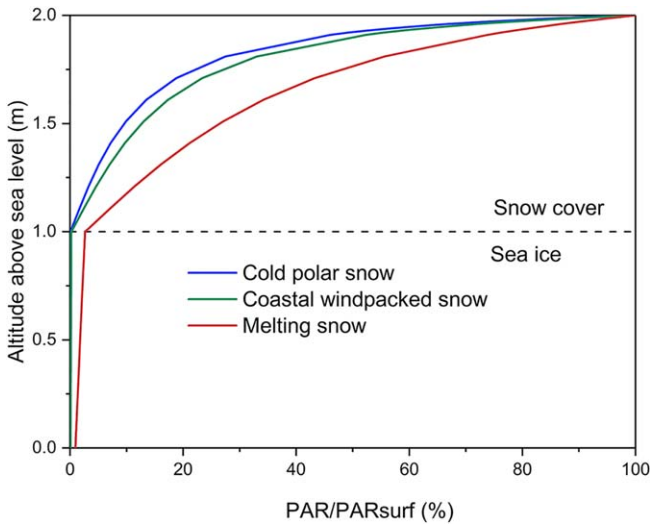

Figure 8. Modeled downwelling irradiance (PAR) through the snow and ice (1 + 1 m) with three different snow types. The plot shows the importance of snow optical properties on the light attenuation and penetration to beneath the sea ice; where Cold Polar, Coastal windpacked, and Melting snow gave irradiance of 0.235, 0.645, and 7.067 μmol photons m^{-2} s^{-1}, respectively, immediately beneath the sea ice.

3.5. Radiative-Transfer Modeling

A radiative-transfer model, TUV-snow, was used to compute the downwelling PAR through a combined snow and sea ice to analyze if changing snow conditions could explain the empirical observations. Specifically, if a change in the optical properties of the snowpack by

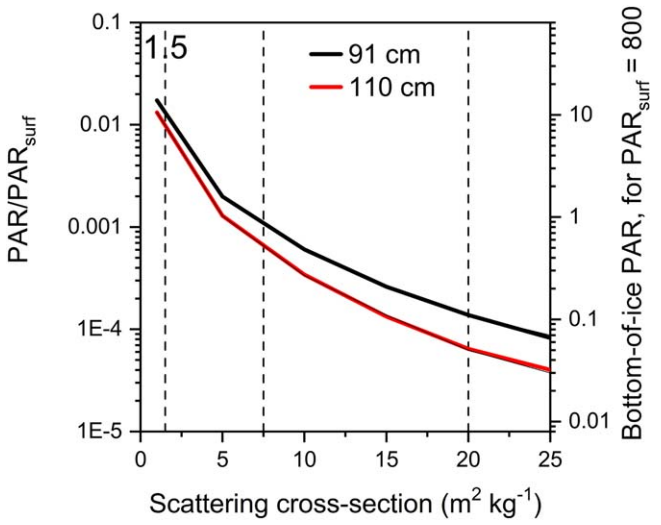

Figure 9. Effect of the optical scattering cross section of snow on the transmittance properties and the light availability beneath the sea ice (relative PAR) at snow thickness of 91 and 110 cm, respectively.

metamorphism could increase the PAR at the bottom of the ice, as previously suggested by Mundy et al. (2005). Figure 8 shows how the amount of PAR within snow and sea ice decreases with depth relative to a surface PAR (plot in relative units). The figure particularly demonstrates that the snowpack is the most attenuating medium compared to the sea ice, and demonstrates how the amount of the light reaching the bottom of the sea ice is dependent on the type of snowpack. Three characteristic snowpacks are shown; i.e., Cold Polar snow, Coastal Windpacked snow, and Melting snow (Lamare et al., 2016). The figure also demonstrates that the difference between the snowpacks can achieve appreciable differences in PAR reaching the snow ice interface (y = 1.0) and the bottom of the sea ice (y = 0). PAR at the bottom of the sea ice varies by at least an order of magnitude, just by considering reasonable changes in the snowpack optical properties.

The amount of light scattering within the snowpack can be assessed by the metric of the light scattering length of the snowpack, equal to the reciprocal product of the light scattering cross section and the snowpack density. Thus, as the light scattering cross section increases the scattering length of the snowpack decreases. Figure 9 demonstrates that changing the properties of the snowpack and thus changing the light scattering length drastically changes the amount of PAR reaching the bottom of the sea ice. The PAR at the sea ice bottom increases as the light scattering length increases (and scattering cross section decreases). In physical terms as the season progresses, snow metamorphoses increases, with a subsequent increase in grain size, and decrease in the light scattering length and light scattering cross section, facilitating an increased PAR flux to the bottom of the sea ice.

The vertical dashed lines on Figure 9 represent three characteristic snow packs, (cold polar, coastal windpack and melting snow). These characteristic snowpacks are based on extensive combined field and modeling work with the radiative-transfer model described here exploring the penetration depth (the e-folding depth) of light in many different snowpacks (Beine et al., 2012; France & King, 2012; France et al., 2011, 2012; Marks & King, 2014). The e-folding depth is the distance over which initial light irradiance within the snowpack decreases to 1/e of its initial value (~37%). Other field studies have also demonstrated the changing snow conditions results in different snow e-folding depths (Galbavy et al., 2007; Libois et al., 2014; Warren, 1982).

Cold polar snowpacks have large values of scattering cross sections and relative short light penetration depths, whilst melting snow has small values of the scattering cross section and large light penetration depths. Each characteristic snowpack has almost one order of magnitude different value of PAR at the base of the sea ice. Thus, the radiative-transfer modeling demonstrated that it is entirely plausible that PAR at the base of sea ice increased due to a change in the snow optical properties owing to the metamorphism of the snowpack.

The low light requirement for algae growth allows earlier productivity by Arctic ice algae than has been recognized before, with consequences for the spatial and temporal distribution of ice algae blooming in Arctic first-year sea ice. Moreover, it has implications for modeling Arctic primary productivity and calculate carbon budgets (Vancoppenolle et al., 2013). This modeling is in agreement with recent observations documenting that phytoplankton blooms underneath sea ice are becoming more abundant (Arrigo et al., 2012; Mundy et al., 2014) even with the presence of snow cover on the ice (Assmy et al., 2017).

5. Conclusions

In this study we have documented the initial phase of ice algae spring growth, beginning under extremely low light conditions (PAR <0.15 μmol photons m^{-2} s^{-1}). This occurred below >1 m thick sea ice covered with ~1 m of windpacked snow in landfast first-year sea ice at NE Greenland (N 81.7°). It confirms observations that ice algae require very little light to support growth and initiate a colonization, and suggests an even lower compensation irradiance than previously anticipated. Furthermore, these findings indicate that

primary production beneath snow-covered first-year sea ice may occur to a greater extent in high latitude Arctic areas and may contribute more substantially to the overall primary production of the Arctic ocean. Using numerical modeling and empirical data we have demonstrated that a change in the optical properties of snow can change the available light underneath sea ice by an order of magnitude, and that snow optical properties can be just as important as the thickness of the snow cover. This has implications for the minimum light requirement for photosynthetic activity and ice algae growth in the wider Arctic. The general thinning of the snow thickness and the sea ice in the Arctic will likely stimulate an increase in ice algae biomass and productivity, and possibly the spring bloom will initiate even earlier than forecasted; with possible implications for light absorption, Arctic primary production, and carbon turnover.

Acknowledgments
We thank the Department of Environmental Science, Aarhus University for providing logistics at Villum Research Station (VRS) in North Greenland, and for access to the monitoring data of solar radiation and snow depth. We also gratefully acknowledge the contributions from Arctic Research Centre (ARC), Aarhus University in supporting the field campaign. This work is a contribution to the Arctic Science Partnership (ASP) asp-net.org. We are very grateful for the highly-qualified assistance in the field at VRS, particularly Bjarki Friis, Ivali Lennert, Kunuk Lennert, and Jesper Hoffman, and the research teams at VRS. We owe the staff at the 'Station Nord' Danish military unit a grateful thank you for assistance with scientific sampling and maintenance of equipment. We appreciate the constructive comments by Andrew McMinn and an anonymous reviewer that improved the manuscript. Data are available from the figshare data repository at (https://figshare.com/s/b0267b2763bbed430387). Financial support is acknowledged to KH, LCLH, and BKS from the Danish Council for Independent Research (Project DFF – 1323-00335: Sea ice ecosystems: Ecological effects of a thinning snow cover) and Carlsberg Foundation Project CF14–0888. MDK and MLL thank NERC for support via grant NE/K00077OX/1.

References

Alou-Font, E., Mundy, C. J., Roy, S., Gosselin, M., & Agusti, S. (2013). Snow cover affects ice algal pigment composition in the coastal Arctic Ocean during spring. *Marine Ecology Progress Series*, *474*, 89. https://doi.org/10.3354/meps10107

Arrigo, K. R. (2014). Sea ice ecosystems. *Annual Review of Marine Sciences*, *6*, 439–467. https://doi.org/10.1146/annurev-marine-010213-135103

Arrigo, K. R., Perovich, D. K., Pickart, R. S., Brown, Z. W., van Dijken, G. L., Lowry, K. E., et al. (2012). Massive phytoplankton blooms under Arctic Sea ice. *Science*, *336*(6087), 1408. https://doi.org/10.1126/science.1215065

Assmy, P., Ehn, J. K., Fernández-Méndez, M., Hop, H., Katlein, C., Sundfjord, A., et al. (2013). Floating ice-algal aggregates below melting Arctic Sea ice. *Plos One*, *8*(10), e76599. https://doi.org/10.1371/journal.pone.0076599

Assmy, P., Fernández-Méndez, M., Duarte, P., Meyer, A., Randelhoff, A., Mundy, C. J., et al. (2017). Leads in Arctic pack ice enable early phytoplankton blooms below snow-covered sea ice. *Scientific Reports-UK*, *7*, 40850. https://doi.org/10.1038/srep40850

Beine, H., Anastasio, C., Domine, F., Douglas, T., Barret, M., France, J., et al. (2012). Soluble chromophores in marine snow, seawater, sea ice and frost flowers near Barrow, Alaska. *Journal of Geophysical Research*, *117*, D00R15. https://doi.org/10.1029/2011JD016650

Boetius, A., Albrecht, S., Bakker, K., Bienhold, C., Felden, J., Fernández-Méndez, M., et al. (2013). Export of algal biomass from the melting Arctic Sea ice. *Science*, *339*(6126), 1430–1432. https://doi.org/10.1126/science.1231346

Braman, R. S., & Hendrix, S. A. (1989). Nanogram nitrite and nitrate determination in environmental and biological-materials by Vanadium(Iii) reduction with chemi-luminescence detection. *Analytical Chemistry*, *61*(24), 2715–2718. https://doi.org/10.1021/ac00199a007

Campbell, K., Mundy, C. J., Barber, D. G., & Gosselin, M. (2014). Remote Estimates of Ice Algae Biomass and Their Response to Environmental Conditions during Spring Melt. *Arctic*, *67*(3), 375–387.

Campbell, K., Mundy, C. J., Barber, D. G., & Gosselin, M. (2015). Characterizing the sea ice algae chlorophyll a-snow depth relationship over Arctic spring melt using transmitted irradiance. *Journal of Marine Systems*, *147*, 76–84. https://doi.org/10.1016/j.jmarsys.2014.01.008

Campbell, K., Mundy, C. J., Landy, J. C., Delaforge, A., Michel, C., & Rysgaard, S. (2016). Community dynamics of bottom-ice algae in Dease Strait of the Canadian Arctic. *Progress in Oceanography*, *149*, 27–39. https://doi.org/10.1016/j.pocean.2016.10.005

Colbeck, S. C. (1982). An overview of seasonal snow metamorphism. *Review of Geophysics* , *20*, 45–61.

Cota, G. F., & Horne, E. P. W. (1989). Physical control of Arctic ice algal production. *Marine Ecology Progress Series*, *52*(2), 111–121. https://doi.org/10.3354/meps052111

Day, J. J., Bamber, J. L., & Valdes, P. J. (2013). The Greenland Ice Sheet's surface mass balance in a seasonally sea ice-free Arctic. *Journal of Geophysical Research: Earth*, *118*, 1533–1544. https://doi.org/10.1002/jgrf.20112

Dmitrenko, I. A., Kirillov, S. A., Rudels, B., Babb, D. G., Pedersen, L. T., Rysgaard, S., et al. (2016). First oceanographic observations on the Wandel Sea shelf in Northeast Greenland: Tracing the Arctic Ocean outflow through the western Fram Strait, *EGU General Assembly Conference Abstracts*, *18*, 1006.

Doherty, S. J., Warren, S. G., Grenfell, T. C., Clarke, A. D., & Brandt, R. E. (2010). Light-absorbing impurities in Arctic snow. *Atmospheric Chemistry and Physics* , *10*(23), 11647–11680. https://doi.org/10.5194/acp-10-11647-2010

Ehn, J. K., & Mundy, C. J. (2013). Assessment of light absorption within highly scattering bottom sea ice from under-ice light measurements: Implications for Arctic ice algae primary production. *Limnology and Oceanography: Methods*, *58*(3), 893–902. https://doi.org/10.4319/lo.2013.58.3.0893

Fernandez-Mendez, M., Wenzhofer, F., Peeken, I., Sorensen, H. L., Glud, R. N., & Boetius, A. (2014). Composition, buoyancy regulation and fate of ice algal aggregates in the central Arctic ocean. *Plos One*, *9*(9), e107452. https://doi.org/10.1371/journal.pone.0107452

France, J. L., & King, M. D. (2012). The effect of measurement geometry on recording solar radiation attenuation in snowpack (e-folding depth) using fibre-optic probes. *Journal of Glaciology*, *58*(208), 417–418. https://doi.org/10.3189/2012JoG11J227

France, J. L., King, M. D., Lee-Taylor, J., Beine, H. J., Ianniello, A., Domine, F., & MacArthur, A. (2011). Calculations of in-snow NO2 and OH radical photochemical production and photolysis rates: A field and radiative-transfer study of the optical properties of Arctic (Ny-Alesund, Svalbard) snow. *Journal of Geophysical Research*, *116*, F04013. https://doi.org/10.1029/2011JF002019

France, J. L., Reay, H. J., King, M. D., Voisin, D., Jacobi, H. W., Domine, F., et al. (2012). Hydroxyl radical and NOx production rates, black carbon concentrations and light-absorbing impurities in snow from field measurements of light penetration and nadir reflectivity of onshore and offshore coastal Alaskan snow. *Journal of Geophysical Research*, *117*, D00R12. https://doi.org/10.1029/2011JD016639

Galbavy, E. S., Anastasio, C., Lefer, B. L., & Hall, S. R. (2007). Light penetration in the snowpack at Summit, Greenland. Part 1. Nitrite and hydrogen peroxide photolysis. *Atmos. Environ*, *41*, 5077–5090. https://doi.org/10.1016/j.atmosenv.2006.04.072

Genty, B., Briantais, J. M., & Baker, N. R. (1989). The relationship between the quantum yield of photosynthetic electron-transport and quenching of chlorophyll fluorescence. *Biochimica et Biophysica Acta*, *990*(1), 87–92.

Glud, R. N., Rysgaard, Kühl, S. M., & Hansen, J. W. (2007). The sea-ice in Young sound: Implications for carbon cycling. In: S. Rysgaard & R. N. Glud (Eds.) *Carbon cycling in Arctic marine ecosystems: Case study Young Sound* (Meddr Greenland , pp. 62–85). Bioscience Special Issue.

Gosselin, M., Legendre, L., Therriault, J. C., & Demers, S. (1990). Light and nutrient limitation of sea-ice microalgae (Hudson-Bay, Canadian Arctic). *Journal of Phycology*, *26*(2), 220–232. https://doi.org/10.1111/j.0022-3646.1990.00220.x

Gosselin, M., Legendre, L., Therriault, J. C., Demers, S., & Rochet, M. (1986). Physical control of the horizontal patchiness of sea-ice microalgae. *Marine Ecology Progress Series*, *29*(3), 289–298. https://doi.org/10.3354/meps029289

Grasshoff, K., Ehrhardt, M., & Kremling, K. (1999). *Methods of seawater analysis* (3rd ed., 600. pp.). Weinheim, Germany: Verlag Chemie GmbH.

Hancke, K., Dalsgaard, T., Sejr, M. K., Markager, S., & Glud, R. N. (2015). Phytoplankton productivity in an Arctic Fjord (West Greenland): Estimating electron requirements for carbon fixation and oxygen production. *Plos One*, *10*(7), e0133275. https://doi.org/10.1371/journal.pone.0133275

Hancke, K., Hancke, T. B., Olsen, L. M., Johnsen, G., & Glud, R. N. (2008). Temperature effects on microalgal photosynthesis-light responses measured by O_2 production, pulse-amplitude-modulated fluorescence, and ^{14}C assimilation. *Journal of Phycology*, *44*(2), 501–514. https://doi.org/10.1111/j.1529-8817.2008.00487.x

Hawes, I., Lund-Hansen, L. C., Sorrell, B. K., Nielsen, M. H., Borzak, R., & Buss, I. (2012). Photobiology of sea ice algae during initial spring growth in Kangerlussuaq, West Greenland: Insights from imaging variable chlorophyll fluorescence of ice cores. *Photosynthesis Research*, *112*(2), 103–115. https://doi.org/10.1007/s11120-012-9736-7

Horner, R., & Schrader, G. C. (1982). Relative contributions of ice algae, phytoplankton, and benthic microalgae to primary production in nearshore regions of the Beaufort Sea. *Arctic*, *35*(4), 485–503.

Jackson, K., Wilkinson, J., Maksym, T., Meldrum, D., Beckers, J., Haas, C., & Mackenzie, D. (2013). A novel and low-cost sea ice mass balance buoy. *Journal of Atmospheric and Oceanic Technology*, *30*(11), 2676–2688. https://doi.org/10.1175/JTECH-D-13-00058.1

Kirk, J. T. O. (1994). *Light and photosynthesis in aquatic ecosystems* (2nd ed.). Bristol, UK: Cambridge University Press.

Krabill, W., Abdalati, W., Frederick, E., Manizade, S., Martin, C., Sonntag, J., et al. (2000). Greenland ice sheet: High-elevation balance and peripheral thinning. *Science*, *289*(5478), 428–430. https://doi.org/10.1126/science.289.5478.428

LaChapelle, E. R. (1969). *Field guide to snow crystals* (101 p.). Seattle, WA: University of Washington Press.

Lamare, M. L., Lee-Taylor, J., & King, M. D. (2016). The impact of atmospheric mineral aerosol deposition on the albedo of snow & sea ice: Are snow and sea ice optical properties more important than mineral aerosol optical properties? *Atmospheric Chemistry and Physics*, *16*(2), 843–860. https://doi.org/10.5194/acp-16-843-2016

Lee-Taylor, J., & Madronich, S. (2002). Calculation of actinic fluxes with a coupled atmosphere-snow radiative transfer model. *Journal of Geophysical Research*, *107*(D24), 4796. https://doi.org/10.1029/2002JD002084

Leu, E., Mundy, C. J., Assmy, P., Campbell, K., Gabrielsen, T. M., Gosselin, M., et al. (2015). Arctic spring awakening - Steering principles behind the phenology of vernal ice algal blooms. *Progress in Oceanography*, *139*, 151–170. https://doi.org/10.1016/j.pocean.2015.07.012

Leu, E., Soreide, J. E., Hessen, D. O., Falk-Petersen, S., & Berge, J. (2011). Consequences of changing sea-ice cover for primary and secondary producers in the European Arctic shelf seas: Timing, quantity, and quality. *Progress in Oceanography*, *90*(1–4), 18–32. https://doi.org/10.1016/j.pocean.2011.02.004

Leu, E., Wiktor, J., Soreide, J. E., Berge, J., & Falk-Petersen, S. (2010). Increased irradiance reduces food quality of sea ice algae. *Marine Ecology Progress Series*, *411*, 49–60. https://doi.org/10.3354/meps08647

Libois, Q., Picard, G., Arnaud, L., Morin, S., & Brun, E. (2014). Modeling the impact of snow drift on the decameter-scale variability of snow properties on the Antarctic Plateau. *Journal of Geophysical Research: Atmospheres*, *119*, 11662–11681. https://doi.org/10.1002/2014JD022361

Libois, Q., Picard, G., France, J. L., Arnaud, L., Dumont, M., Carmagnola, C. M., & King, M. D. (2013). Influence of grain shape on light penetration in snow. *Cryosphere*, *7*(6), 1803–1818. https://doi.org/10.5194/tc-7-1803-2013

Littler, M. M., Littler, D. S., Blair, S. M., & Norris, J. N. (1985). Deepest known plant life discovered on an uncharted seamount. *Science*, *227*(4682), 57–59. https://doi.org/10.1126/science.227.4682.57

Littler, M. M., Littler, D. S., Blair, S. M., & Norris, J. N. (1986). Deep-water plant-communities from an uncharted seamount off San Salvador Island, Bahamas - distribution, abundance, and primary productivity. *Deep-Sea Research Part A-–Oceanographic Research Papers*, *33*(7), 881–892. https://doi.org/10.1016/0198-0149(86)90003-8

Littler, M. M., Littler, D. S., & Hanisak, M. D. (1991). Deep-water Rhodolith distribution, productivity, and growth history at sites of formation and subsequent degradation. *Journal of Experimental Marine Biology and Ecology*, *150*(2), 163–182. https://doi.org/10.1016/0022-0981(91)90066-6

Lorenzen, C. J. (1966). A method for the continuous measurement of in vivo chlorophyll concentration. *Deep-Sea Research Part A-–Oceanographic Research Papers*, *13*, 223–227.

Lund-Hansen, L. C., Hawes, I., Nielsen, M. H., & Sorrell, B. K. (2016). Is colonization of sea ice by diatoms facilitated by increased surface roughness in growing ice crystals? *Polar Biology*. https://doi.org/10.1007/s00300-016-1981-3

Lund-Hansen, L. C., Hawes, I., Sorrell, B. K., & Nielsen, M. H. (2014). Removal of snow cover inhibits spring growth of Arctic ice algae through physiological and behavioral effects. *Polar Biology*, *37*(4), 471–481. https://doi.org/10.1007/s00300-013-1444-z

Lund-Hansen, L. C., Markager, S., Hancke, K., Stratmann, T., Rysgaard, S., Ramiov, H., & Sorrell, B. K. (2015). Effects of sea-ice light attenuation and CDOM absorption in the water below the Eurasian sector of central Arctic Ocean (> 88 degrees N). *Polar Research*, *34*, 23978.

Marks, A. A., & King, M. D. (2014). The effect of snow/sea ice type on the response of albedo and light penetration depth (e-folding depth) to increasing black carbon. *Cryosphere*, *8*(5), 1625–1638. https://doi.org/10.5194/tc-8-1625-2014

Marra, J. (2004). The compensation irradiance for phytoplankton in nature. *Geophysical Research Letters*, *31*, L06305. https://doi.org/10.1029/2003GL018881

McMinn, A., Ashworth, C., & Ryan, K. G. (2000). In situ net primary productivity of an Antarctic fast ice bottom algal community. *Aquatic Microbial Ecology*, *21*(2), 177–185. https://doi.org/10.3354/ame021177

McMinn, A., Pankowskii, A., Ashworth, C., Bhagooli, R., Ralph, P., & Ryan, K. (2010). In situ net primary productivity and photosynthesis of Antarctic sea ice algal, phytoplankton and benthic algal communities. *Marine Biology*, *157*(6), 1345–1356. https://doi.org/10.1007/s00227-010-1414-8

Mikkelsen, D. M., Rysgaard, S., & Glud, R. N. (2008). Microalgal composition and primary production in Arctic sea ice: A seasonal study from Kobbeijord (Kangerluarsunnguaq), West Greenland. *Marine Ecology Progress Series*, *368*, 65–74. https://doi.org/10.3354/meps07627

Mock, T., & Gradinger, R. (2000). Changes in photosynthetic carbon allocation in algal assemblages of Arctic sea ice with decreasing nutrient concentrations and irradiance. *Marine Ecology Progress Series*, *202*, 1–11.

Mundy, C. J., Barber, D. G., & Michel, C. (2005). Variability of snow and ice thermal, physical and optical properties pertinent to sea ice algae biomass during spring. *Journal of Marine Systems*, *58*(3–4), 107–120. https://doi.org/10.1016/j.jmarsys.2005.07.003

Mundy, C. J., Ehn, J. K., Barber, D. G., & Michel, C. (2007). Influence of snow cover and algae on the spectral dependence of transmitted irradiance through Arctic landfast first-year sea ice. *Journal of Geophysical Research*, *112*, C03007. https://doi.org/10.1029/2006JC003683

Mundy, C. J., Gosselin, M., Gratton, Y., Brown, K., Galindo, V., Campbell, K., et al. (2014). Role of environmental factors on phytoplankton bloom initiation under landfast sea ice in Resolute Passage, Canada, *Marine Ecology Progress Series*, *497*, 39. https://doi.org/10.3354/meps10587

Palmisano, A. C., & Sullivan, C. W. (1983). Sea ice microbial communities (Simco). 1. Distribution, abundance, and primary production of ice microalgae in Mcmurdo-Sound, Antarctica in 1980. *Polar Biology*, *2*(3), 171–177. https://doi.org/10.1007/BF00448967

Pritchard, D. W., Hurd, C. L., Beardall, J., & Hepburn, C. D. (2013). Survival in low light: Photosynthesis and growth of a red alga in relation to measured in situ irradiance. *Journal of Phycology*, *49*(5), 867–879. https://doi.org/10.1111/jpy.12093

Raven, J. A., Kubler, J. E., & Beardall, J. (2000). Put out the light, and then put out the light. *Journal of the Marine Biological Association of the United Kingdom*, *80*(1), 1–25. https://doi.org/10.1017/S0025315499001526

Robinson, D. H., Arrigo, K. R., Iturriaga, R., & Sullivan, C. W. (1995). Microalgal light-harvesting in extreme low-light environments in Mcmurdo Sound, Antarctica. *Journal of Phycology*, *31*(4), 508–520. https://doi.org/10.1111/j.1529-8817.1995.tb02544.x

Robinson, D. H., Kolber, Z., & Sullivan, C. W. (1997). Photophysiology and photoacclimation in surface sea ice algae from McMurdo Sound, Antarctica. *Marine Ecology Progress Series*, *147*(1–3), 243–256. https://doi.org/10.3354/meps147243

Rysgaard, S., & Glud, R. N. (2007). Carbon cycling and climate change: Predictions for a High Arctic marine ecosystem (Young Sound, NE Greenland). *Meddelelser om Gronland Bioscience*, *58*, 205–214.

Rysgaard, S., Kuhl, M., Glud, R. N., & Hansen, J. W. (2001). Biomass, production and horizontal patchiness of sea ice algae in a high-Arctic fjord (Young Sound, NE Greenland). *Marine Ecology Progress Series*, *223*, 15–26.

Schreiber, U., Schliwa, U., & Bilger, W. (1986). Continuous recording of photochemical and nonphotochemical chlorophyll fluorescence quenching with a new type of modulation fluorometer. *Photosynthesis Research*, *10*(1–2), 51–62.

Simpson, W. R., King, M. D., Beine, H. J., Honrath, R. E., & Zhou, X. L. (2002). Radiation-transfer modeling of snow-pack photochemical processes during ALERT 2000. *Atmospheric Environment*, *36*(15–16), 2663–2670. https://doi.org/10.1016/S1352-2310(02)00124-3

Soreide, J. E., Leu, E., Berge, J., Graeve, M., & Falk-Petersen, S. (2010). Timing of blooms, algal food quality and Calanus glacialis reproduction and growth in a changing Arctic. *Global Change Biology*, *16*(11), 3154–3163. https://doi.org/10.1111/j.1365-2486.2010.02175.x

Stamnes, K., Tsay, S. C., Wiscombe, W., & Jayaweera, K. (1988). Numerically stable algorithm for discrete-ordinate-method radiative-transfer in multiple-scattering and emitting layered media. *Applied Optics*, *27*(12), 2502–2509.

Thomas, D. N., & Dieckmann, G. S. (2009). *Sea ice*. Wiley-Blackwell.

Vancoppenolle, M., Bopp, L., Madec, G., Dunne, J., Ilyina, T., Halloran, P. R., & Steiner, N. (2013). Future Arctic Ocean primary productivity from CMIP5 simulations: Uncertain outcome, but consistent mechanisms. *Global Biogeochemical Cycles*, *27*, 605–619. https://doi.org/10.1002/gbc.20055

Warren, S. G. (1982). Optical-properties of snow. *Review of Geophysics*, *20*, 67–89. https://doi.org/10.1029/RG020i001p00067

Warren, S. G., & Brandt, R. E. (2008). Optical constants of ice from the ultraviolet to the microwave: A revised compilation. *Journal of Geophysical Research*, *113*, D14220. https://doi.org/10.1029/2007JD009744